

Divide migration and escarpment retreat: numerical models and application to the rift margin of Madagascar

Yanyan Wang¹, Sean Willett¹, and Datian Wu²

¹Swiss Federal Institute of Technology in Zurich

²China Geological Survey

November 24, 2022

Abstract

A great escarpment at a rift margin can correspond directly to a major water divide but at many margins, including in Madagascar, the escarpment often appears as a steep knickzone on rivers that have their main water divides in the interior of the high plateau. We hypothesize that this variability in morphology is a reflection of the frequency and size of drainage area captured from the high plateau over the escarpment. To test this hypothesis, we document morphological features and weathering conditions from river sediment of Madagascar. We propose that the existence of a weathered weak surface layer of crystalline bedrock encourages large river captures from the upper plateau, leading to a dominance of knickpoint type rivers. We demonstrate that this is feasible, using 2-D landscape evolution models and show that an easily-eroded surface layer is prone to fast divide migration through frequent river capture and reversal. A positive scaling relationship between captured area and escarpment retreat rate is found from models. We demonstrate that this scaling is also observed in the great escarpments of Madagascar and India.

1 Divide migration and escarpment retreat: numerical 2 models and application to the rift margin of 3 Madagascar

4 Yanyan Wang¹; Sean D. Willett¹; Datian Wu²

5 ¹ETH Zurich, Department of Earth Sciences, Sonneggstrasse 5, 8092 Zurich, Switzerland.

6 ²China Geological Survey, Shengyang Center, Huanghe North Street 280, 110034 Shenyang,
7 China.

8
9 Corresponding author: Yanyan Wang (yanyan.wang@erdw.ethz.ch)

10 Abstract

11 A great escarpment at a rift margin can correspond directly to a major water divide but at many margins,
12 including in Madagascar, the escarpment often appears as a steep knickzone on rivers that have their main
13 water divides in the interior of the high plateau. We hypothesize that this variability in morphology is a
14 reflection of the frequency and size of drainage area captured from the high plateau over the escarpment.
15 To test this hypothesis, we document morphological features and weathering conditions from river sediment
16 of Madagascar. We propose that the existence of a weathered weak surface layer of crystalline bedrock
17 encourages large river captures from the upper plateau, leading to a dominance of knickpoint type rivers.
18 We demonstrate that this is feasible, using 2-D landscape evolution models and show that an easily-eroded
19 surface layer is prone to fast divide migration through frequent river capture and reversal. A positive scaling
20 relationship between captured area and escarpment retreat rate is found from models. We demonstrate that
21 this scaling is also observed in the great escarpments of Madagascar and India.

22 1 Introduction

23 A great escarpment at a passive margin is generally characterized by asymmetrical topography with a steep
24 escarpment on the edge of a flat plateau, often with the top edge of the escarpment acting as the water divide.
25 Alternatively, the water divide can be found internal to the plateau, at some distance from the steep
26 escarpment. In the latter case, a significant area of the high plateau drains over the escarpment and the
27 escarpment appears in the form of a knickzone on an escarpment river profile. The two morphologically
28 distinct escarpment types have been referred to as “shoulder-type” and “arch-type”, respectively (Bishop,
29 2007; Matmon et al., 2002), to indicate a different geodynamic formation mechanism.

30 The retreat of an escarpment with a water divide at its crest is driven by the differential erosion rates across
31 the water divide where the steep escarpment erodes faster than the relatively slow eroding highland (Braun,
32 2018; Kooi and Beaumont, 1994; Tucker and Slingerland, 1994; Willett et al., 2018). In this case, it is the
33 fluvial incision processes that set the rate of both divide and escarpment retreat, as demonstrated by a
34 number of models (Braun, 2018; Willett et al., 2018). In the case where the water divide is located inland
35 from the escarpment, these models will not apply and it is not clear whether the drainage basin morphology
36 is set by other processes, such as flexural uplift (Tucker and Slingerland, 1994), or if the divide location is
37 a transient feature set by capture of plateau area (Giachetta and Willett, 2018). The capture of highland
38 rivers creates a spatial offset between the major divide and the escarpment, making a local segment of the
39 escarpment appear to have a knickzone as it crosses the escarpment. In the case of isolated river capture
40 with a subsequently stable water divide, the knickzone will migrate upstream returning the form of the river
41 profile to a non-stepped, concave-up profile with the escarpment corresponding to the water divide. In this
42 paper, we will discuss the morphology and genesis of escarpment rivers and will use the terms “divide-
43 type” and “knickzone-type”, to refer to the two morphologically distinct river profiles.

44 River capture is a common occurrence at many escarpments. For example, on the Serra Geral escarpment
45 in southern Brazil, the current escarpment rivers have captured the inland plateau drainages during the

46 retreat, leaving morphological traces of elbows, underfit valleys, and other evidence of river network
47 rearrangement (de Sordi et al., 2018). Fluvial terraces filled with round pebbles are found on the crest of
48 the Blue Ridge escarpment in the Appalachians, implying a capture of big, formerly plateau-confined rivers
49 by the escarpment rivers (Prince et al., 2010). Morphological features of highland rivers and hillslopes
50 might control patterns of captures (frequency and scale). Harel et al. (2019) demonstrated that progressive
51 reversal and capture of highland rivers by escarpment rivers could be facilitated by lithological differences
52 where a softer substrate fills a highland river valley. Harel et al. (2019) proposed a mechanism where
53 windgap/water divide migration is independent of the escarpment retreat, or at least, where they are spatially
54 separated and migrating together.

55 The conventional interpretation of knickpoints on rivers is that they represent temporal or spatial changes
56 in uplift rate or rock erodibility (Gallen, 2018; Kirby and Whipple, 2012). If they are the result of a temporal
57 change in uplift rate, they should propagate upstream, independent of any motion of the water divide.
58 Alternatively, if knickpoints represent widespread river capture due to escarpment retreat (Giachetta and
59 Willett, 2018), their formation and retreat should be linked to the jumps of the water divide. In this case,
60 arch-type escarpments dominated by knickzone-type rivers are not genetically different from shoulder-type
61 escarpments, but are simply a reflection of more common river capture. Such a model is supported by the
62 presence of both types of river profiles on the same escarpment which has been documented, for example,
63 in Madagascar (Wang and Willett, 2021).

64 In this paper, we use data from Madagascar to examine the processes of escarpment retreat by divide
65 migration and river capture. In particular, we investigate the occurrence and frequency of rivers of both
66 knickzone- and divide-type, that is those that exhibit large knickzones and those that terminate at an
67 escarpment-top divide. To explain the large numbers of each type of river profile, we hypothesize that river
68 capture is encouraged by the existence of a thick, easily-eroded, surface layer on the high plateau of
69 Madagascar that is a result of widespread and extensive weathering. We demonstrate that this affects both

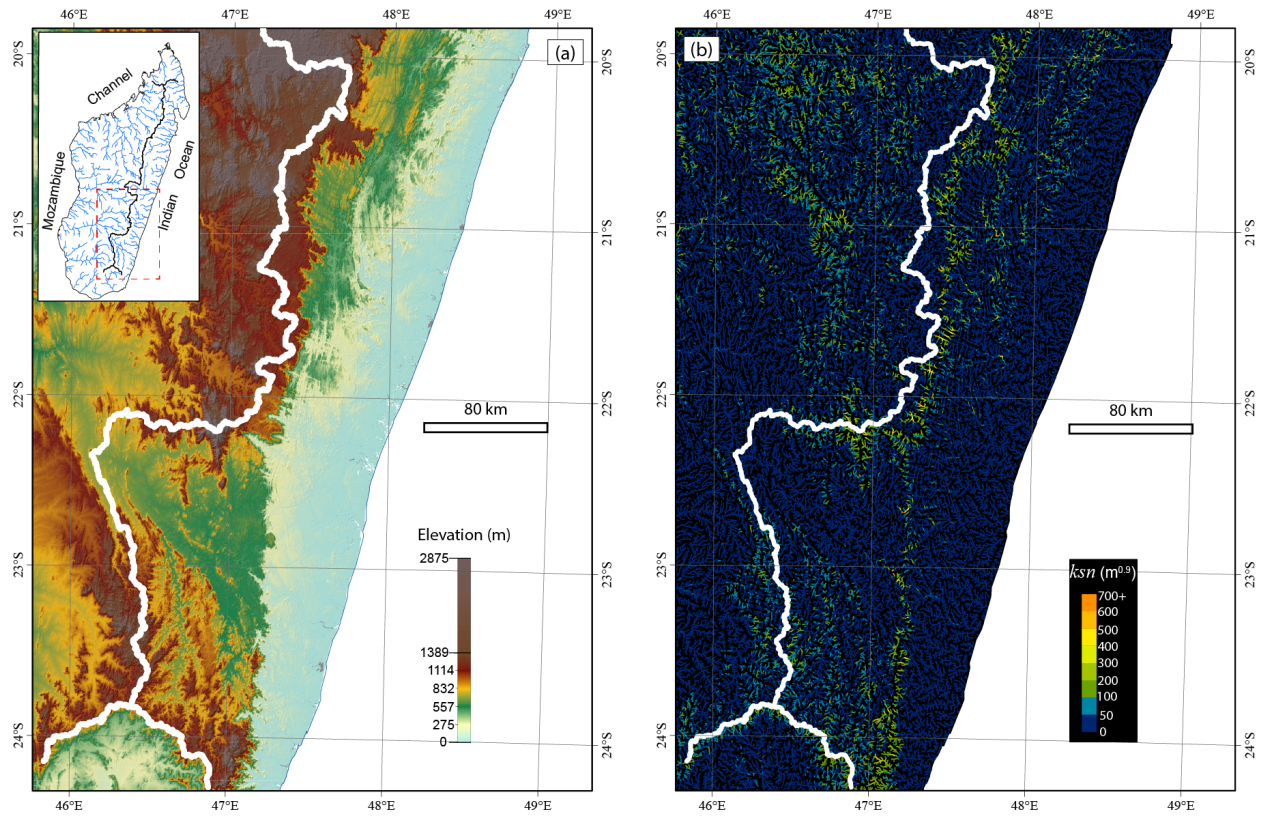
70 the rate of escarpment retreat and the frequency of river captures. We explore these implications with 2-D
71 models of landscape evolution.

72 2 Geomorphic characteristics of the escarpment and water divide of Madagascar

73 2.1 Spatial offset between divide and escarpment

74 A great escarpment is characterized by a high relief zone rimming an inland low-relief, high-elevation
75 plateau. Eastern Madagascar is characterized by a great escarpment that extends inland of the coastal plain
76 for ~1000 km (Gunnell and Harbor, 2008; Wang et al., 2021). The major continental water divide that
77 separates eastern and western flowing rivers approximately follows the top of the escarpment (Fig. 1a and
78 inset). There is a spatial offset between the island divide and the escarpment (Fig. 1a). Although there are
79 times when the divide follows the escarpment, it is, however, not rare for it to be located kilometers to 10s-
80 100s kilometers distant from the escarpment (Fig. 1a). The area between the divide and the escarpment
81 edge is characterized by low-gradient river reaches, similar to the plateau rivers on the other side of the
82 water divide (Fig. 1b). Regardless of where the divide is located, the steep escarpment reaches stand in
83 contrast to both the low-gradient coastal reaches and the plateau reaches of escarpment rivers (Fig. 1b). We
84 summarize the river profile shapes in Fig. 2. Approximately 33% of Madagascar escarpment rivers are
85 knickzone-type, and 57% of rivers are divide-type with the remaining rivers indeterminate at the scale of
86 our analysis (Fig. 2 b-e). The two forms of the river profiles appear almost randomly along the strike of the
87 escarpment with no spatial patterns or long, consistent segments.

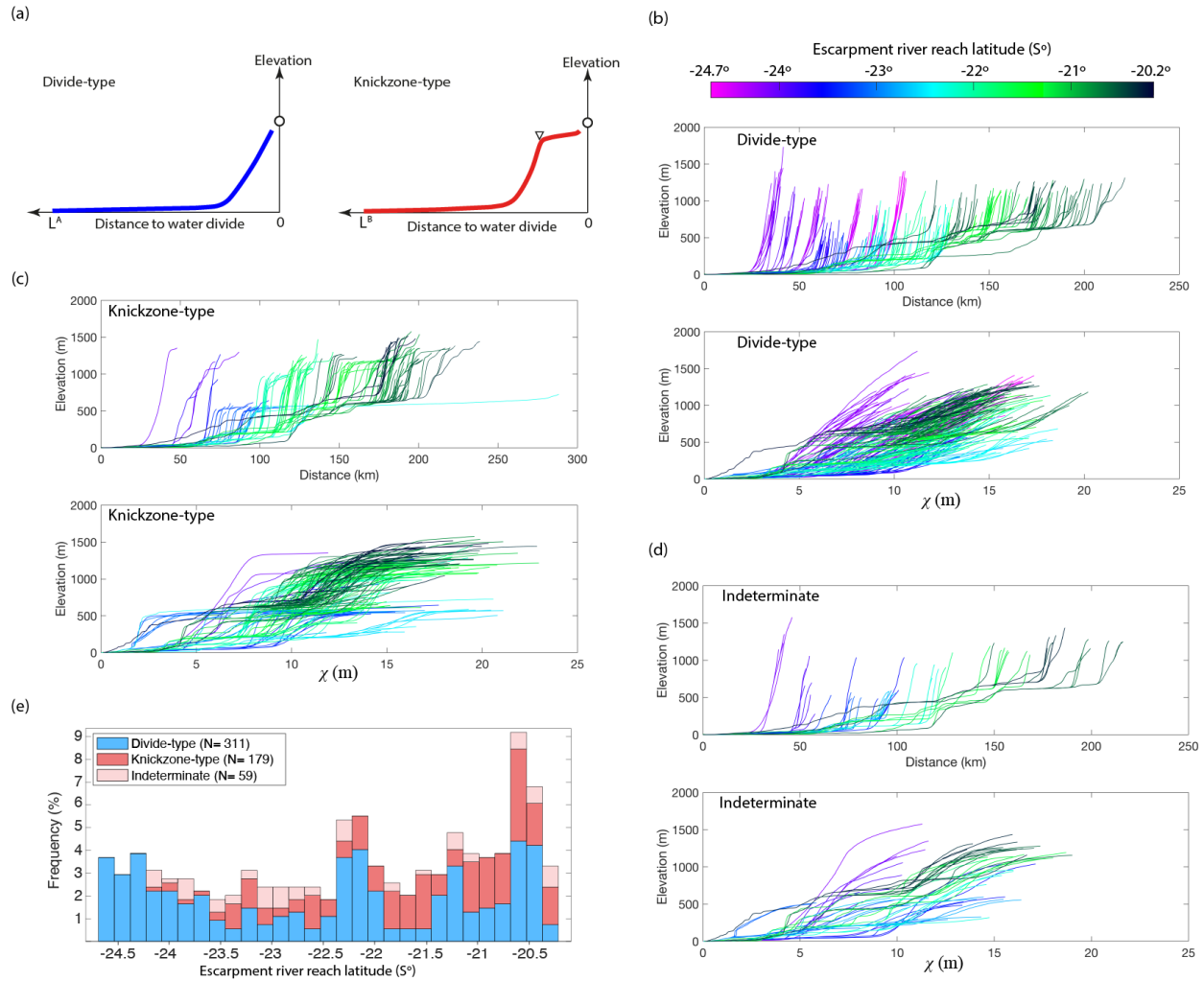
88



89

90 Fig. 1 (a) Topography of Madagascar, with the main water divide in white and major rivers shown in the
 91 inset. (b) Normalized river steepness index (Wobus et al., 2006). The topography is from the Shuttle Radar
 92 Topography Mission (SRTM) 90 m digital elevation model (DEM) (Jarvis et al., 2008). Rivers are extracted
 93 from 90 m HydroSHEDS DEM (Lehner et al., 2008) and clipped to a minimum drainage area of 5 km².

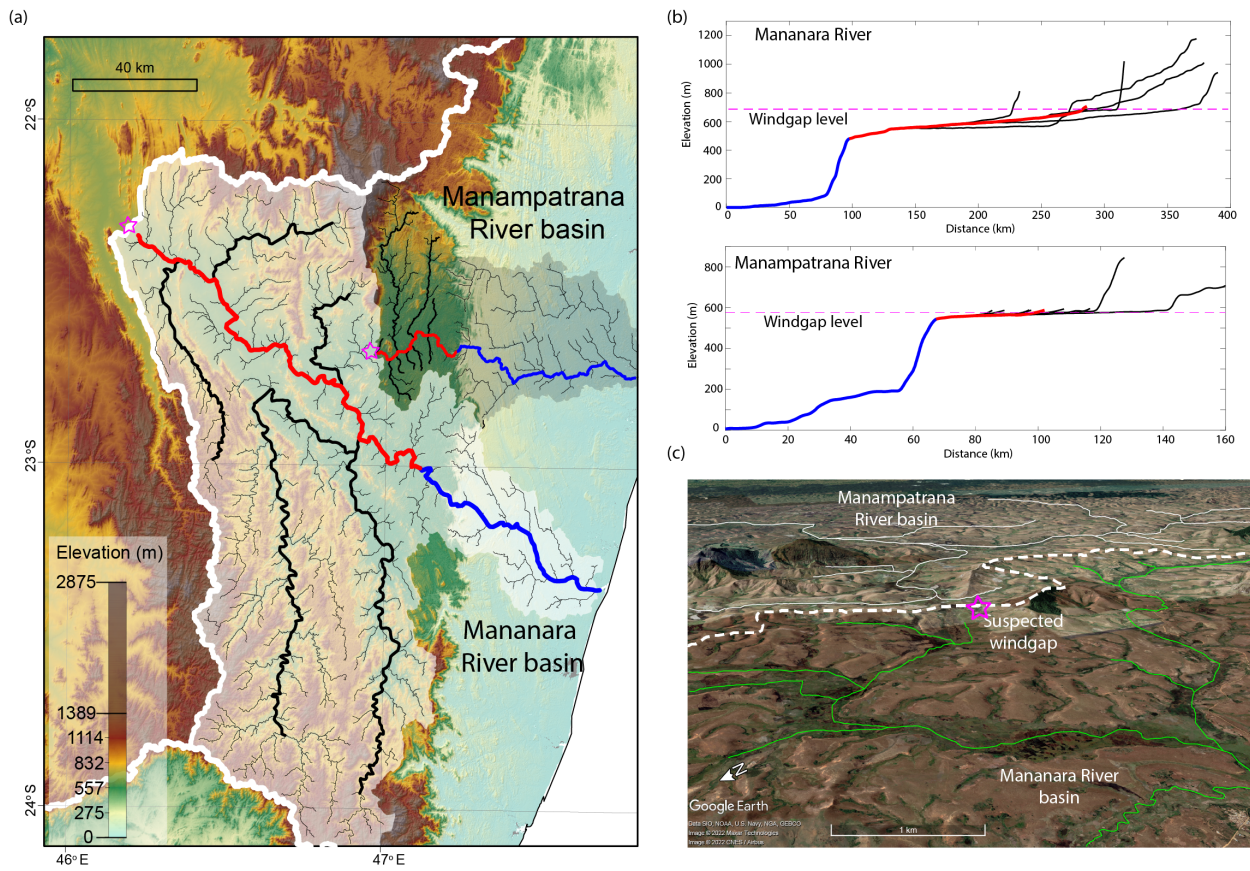
94



97 Fig. 2 Escarpment river types of eastern Madagascar. The location of the studied escarpment is shown in
 98 Fig. 1a. (a) Schematic summary of divide-type and knickzone-type river profiles. (b) Escarpment river
 99 profiles exhibiting divide-type, plotted against distance and normalized distance (Perron and Royden, 2013)
 100 and colored by the latitude of channel head. (c) Escarpment river profiles exhibiting knickzone-type ,
 101 plotted in the same manner as (b). (d) Escarpment river profiles of indeterminate form, plotted in the same
 102 manner as (b). (e) Spatial distribution of escarpment river types along the strike of the great escarpment.

103 2.2 River capture

104 Paleo-captures of highland rivers by escarpment-draining rivers are common in Madagascar. We expect
105 that these occur at multiple scales, and with a variety of patterns of reversal or flow redirection. For example,
106 in southern Madagascar, the capture of the Mananara River has driven the divide ~200 km away from the
107 escarpment (Fig. 3a). Delaunay (2018) and Schreurs et al. (2010) pointed out the water divide of the
108 Mananara River basin is established through captures of three big, and many small, plateau tributaries and
109 reversal of the trunk channel on the flat plain (Fig. 3a). The neighboring Manampatrana River, is also
110 advancing its headwater divide into the plateau with a similar pattern of drainage reversal and progressive
111 capture of tributaries (Fig. 3a). This capture of plateau area could be at the expense of the Mananara, or
112 previously west-flowing rivers, depending on the order of the capture events, which is unknown. The
113 abandoned watercourse at the head of the Manampatrana is identified from Google Earth images and
114 indicated in Fig. 3c. Rivers on top of the plateau in the aggressive escarpment basin are low gradient (Fig.
115 3b) and the junction angles between the tributaries and the trunk channel are usually larger than 90 degrees
116 (Fig. 3a, 3c). Similar situations of capture-driven decoupling of water divides and escarpments are found at
117 other sites along the escarpment.



118

119 Fig. 3 (a) Escarpment-draining basins in southern Madagascar showing major river capture events. Black
 120 lines mark the major captured tributaries where the trunk channels on the plateau (red) are reversed and
 121 captured by the escarpment reach (blue). The thick white line is the island water divide. The Mananara
 122 River basin (shaded in white) is interpreted to be a major capture from west to east-flowing. The
 123 Manampatrana River (shaded in grey) is also interpreted to have captured area that used to be west-flowing.
 124 The stars indicate the identified windgap at the head of the reversed reach. (b) River profiles of the
 125 Mananara and the Manampatrana rivers. (c) Google Earth image showing the abandoned river course
 126 between the Mananara (the green) and the Manampatrana (the white) rivers where the white dashed line
 127 marks the divide between them.

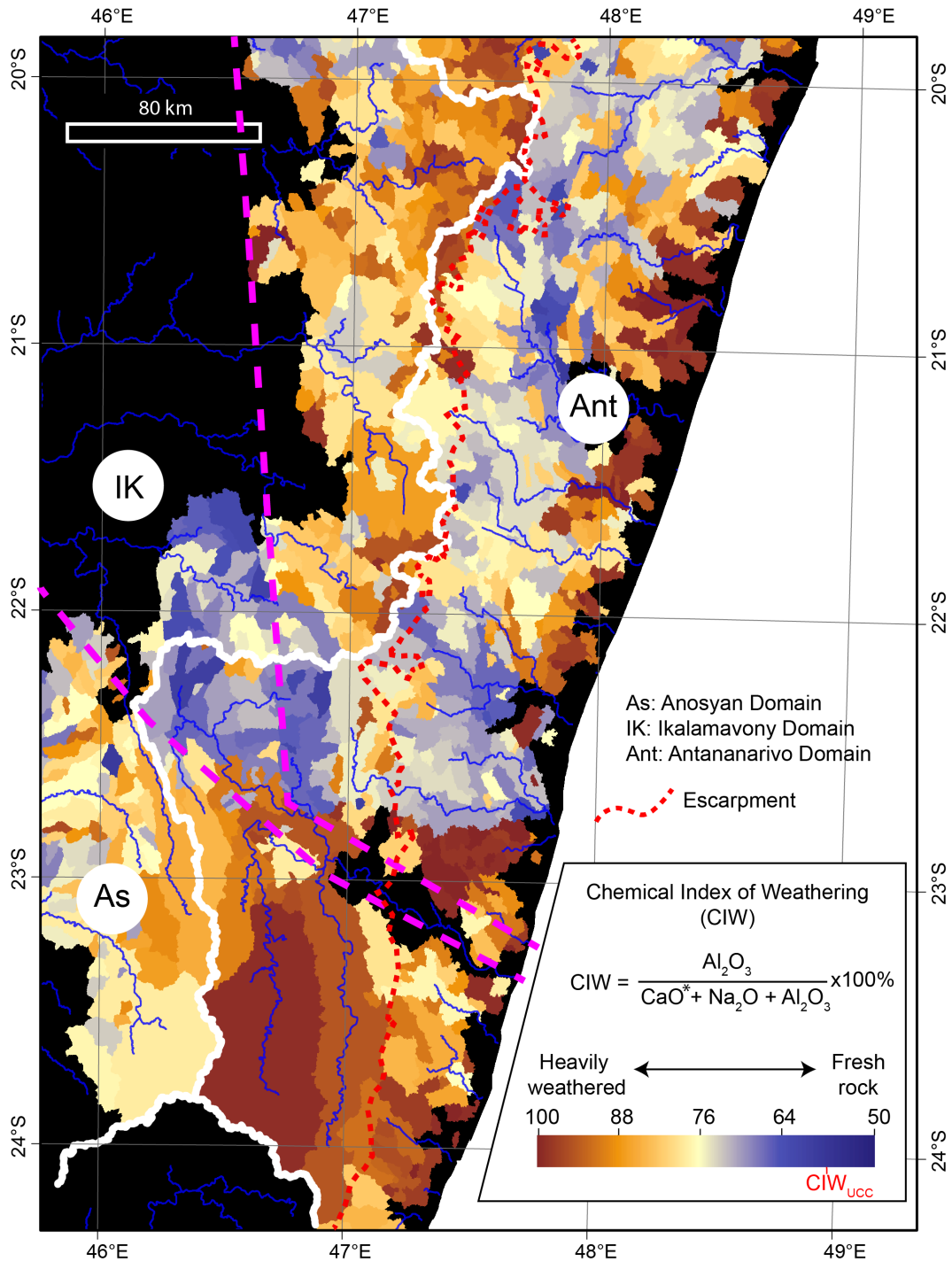
128 2.3 Weathered high plateau of Madagascar

129 The relative weathering intensity of silicate rock can be assessed with the relative abundance of major
130 elements. The relative weathering intensity indices calculated on riverine sediment, especially on suspended
131 sediment, represent the average weathering conditions of a catchment (Guo et al., 2018; Lecomte, 2014).
132 A survey conducted by the China Geological Survey, Shenyang Section, sampled a total of 1136 samples
133 of bedload river sediment in the study area and measured major elements. 90% of the sampled catchments
134 are in the range of 10s-100s km², with 55.5% smaller than 100 km². Samples were sieved to a size fraction
135 below 850 μm , and major elements were measured at the Mineral Resource Supervise Examine Center in
136 Zhengzhou, China. Major elements were measured using XRF (SiO₂ and Al₂O₃) and ICP-MS (CaO, K₂O,
137 MgO, and Na₂O). To estimate the general degree of bedrock weathering, we calculated the commonly used
138 chemical index of weathering (CIW) (Harnois, 1988). High CIW indicates a high degree of weathering.

139 South of the Alaotra-Ankay graben area, the study area comprises three geological domains of the
140 Precambrian shield that are differentiated based on geological age, lithology, climate, and metamorphic
141 fabrics. These are referred to as the Antananarivo, Ikalamavony, and Anosyan domains (Tucker et al., 2014).
142 Our calculated weathering indices indicate differences in the degree of weathering between these geologic
143 domains as well as between the modern morphological domains (Fig. 4). The Antananarivo Domain is
144 intensively weathered on the highland above the escarpment and the coastal plain. The escarpment zone is
145 less weathered. The Ikalamavony Domain shows a low degree of weathering throughout Madagascar. The
146 southernmost Anosyan Domain shows a high degree of weathering, including the escarpment. Other
147 weathering indexes, i.e. the chemical index of alteration, the Plagioclase index of alteration, and the
148 weathering index of Parker show the same weathering pattern as the CIW (Supplement Figures S1-S3).

149 We expect that the CIW reflects the degree of weathering intensity and the thickness of the weathered zone
150 across Madagascar. A thick regolith layer has been described on the highly weathered plateau of
151 Madagascar (Wells et al., 1997; Wells and Andriamihaja, 1993, 1990). This regolith layer is fractured and

152 altered from the crystalline Precambrian bedrock. It acts as an important surface water aquifer for the central
153 plateau of Madagascar (Davies, 2009; Rahobisoa et al., 2014). The relatively weak regolith layer is also
154 manifested from high-density of hillslope failures which excavate up to 10s meters of regolith on the central
155 Madagascar Plateau (Brosens et al., 2022; Cox et al., 2010). We posit that this layer also affects the pattern
156 of river profiles and the frequency of river capture, as we explore in the subsequent section.



157

158 Fig. 4 Chemical index of weathering (CIW) from river sediment of Madagascar. The mean CIW of average
 159 elemental compositions of upper continental crust (CIW_{UCC}) is from Rudnick and Gao (2005). The three
 160 geological domains (As, IK, and Ant) are indicated and are different in age and major lithological
 161 composition (Tucker et al., 2014). Compositional and morphological effects are evident with low CIW in

162 the IK and on the escarpment. Higher values of CIW are observed on both the plateau and the coastal
163 lowlands.

164 3 Modeling of escarpment retreat with an erodible surface layer

165 We hypothesize that the regolith-mantled high plateau of Madagascar has facilitated the many observed
166 captures and the frequency of the knickzone-type Madagascar escarpment rivers. The regolith layer can be
167 generalized as an erosionally weak surface layer. Given the systematic weathering contrast between the
168 high plateau and the escarpment, homogeneous erosion-resistant substrate can be assumed to characterize
169 the substrate of the escarpment and the underlying unweathered bedrock. To test this hypothesis, we
170 construct a series of numerical models of the landscape evolution, including fluvial incision processes with
171 differentially erodible bedrock. We use the Divide and Capture (DAC) landscape evolution model (Goren
172 et al., 2014) which includes an explicit, and therefore a precise representation of water divides and river
173 capture (Goren et al., 2014).

174 3.1 Model set-up

175 To simulate a weak surface layer, we apply a layer covering the entire plateau (Fig. 5). The weak surface
176 layer is characterized by the thickness, T_{hw} , and the erodibility, K_w , both of which are constant in time (Fig.
177 5). The underlying bedrock has a lower erodibility value, K_b . On the plateau side, plateau rivers always
178 incise into the weak layer and given sufficient time or proximity to the escarpment, will incise through the
179 weak layer reaching the more erosion-resistant bedrock. On and below the escarpment, the weak surface
180 layer is not present or fully removed by erosion.

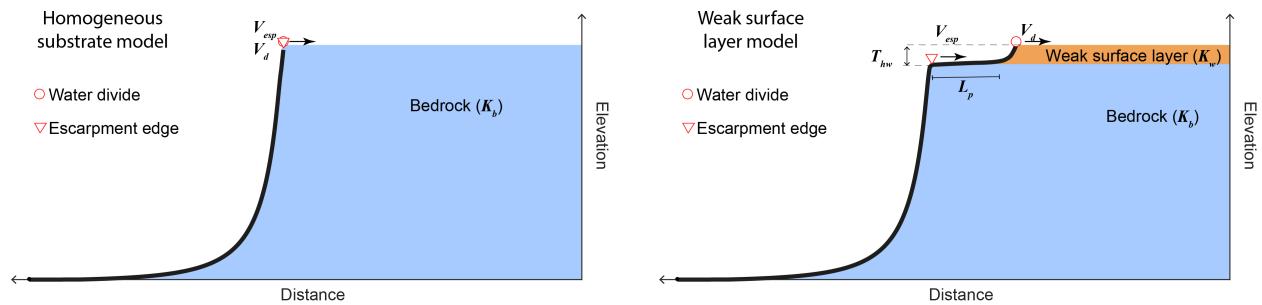
181 The model consists of a two-dimensional domain, representing a planform surface over which water is
182 routed into rivers, which subsequently incise into the substrate following a stream-power law (Whipple and
183 Tucker, 1999):

$$E = KA^m S^n \quad (1)$$

184 The river erosion rate, E , is physically characterized by the shear-stresses on the substrate and the rock
 185 erodibility, K . Shear stress is approximated with the drainage area, A , and channel slope, S . m and n are
 186 empirical parameters. We use the landscape evolution code, DAC, to solve the stream-power equation at
 187 each numerical grid point. DAC calculates water routing and incision and applies geometric rules for river
 188 capture and precise divide positioning (Goren et al., 2014). Regions upstream of a threshold drainage area
 189 are regarded as hillslope dominated and are assigned a steady, threshold slope.

190 We construct a reference escarpment retreat model for comparison with the weak surface layer model. In
 191 the reference model, a uniform erodibility, K_b , is used for all grid nodes throughout time and space.

192



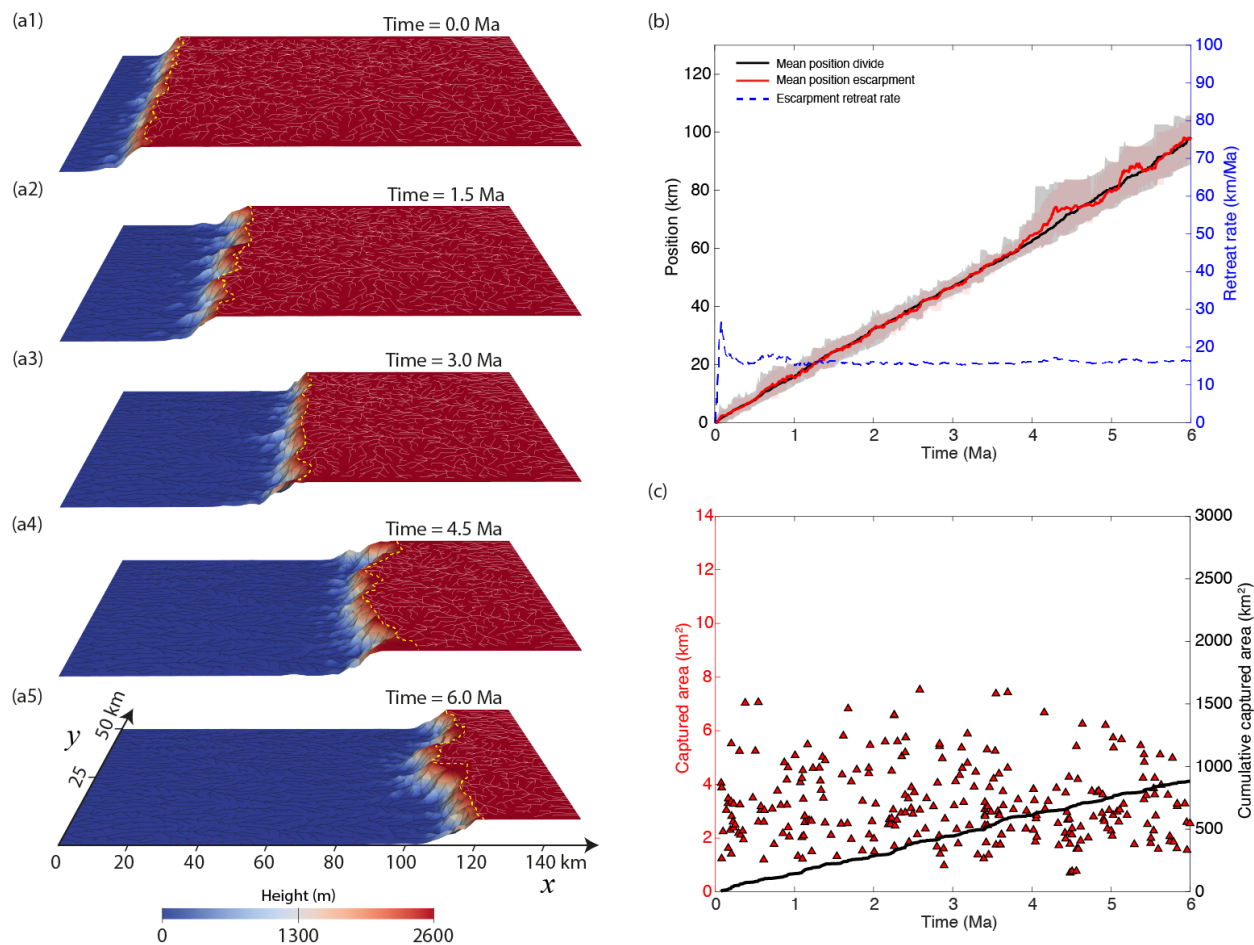
194 Fig. 5 Cross-section view of the reference homogeneous substrate model and the weak surface layer model.
 195 In the weak surface layer model, a surface layer (thickness T_{hw} , erodibility K_w) mantles the highland,
 196 overlying the bedrock (erodibility K_b). The thick black line is a schematic of an escarpment river. The divide
 197 and escarpment retreat at rates of V_d and V_{esp} , respectively.

198 3.2 Results of escarpment retreat model for a homogenous substrate

199 We run a simulation, S0, to study the homogeneous substrate case. The simulation starts from an initial
 200 escarpment landscape and river network (Fig. 6 a1). The initial escarpment rivers are of the divide-type:

201 the top edge of the escarpment acts as the major water divide that separates the plateau rivers and
202 escarpment rivers. The steep reaches of the initial escarpment rivers dictate a regular escarpment front with
203 little sinuosity.

204 In the homogenous substrate model, the escarpment retreats and continues to define the major water divide
205 for most of space and time (Fig. 6 a1-a5, Supplement Movie S1). The position of the major water divide
206 approximately corresponds to the escarpment edge in space (Fig. 6 b), with transient exceptions when a
207 river capture forces a region of the plateau to drain over the escarpment edge, creating a spatial offset
208 between the major divide and the escarpment. On average, the divide and the escarpment retreat steadily
209 both temporally and spatially as predicted by theory (Braun, 2018; Willett et al., 2018) (Fig. 6 b). The
210 escarpment front is regular, although more sinuous than the initial condition. Sinuosity is transient,
211 reflecting the occurrence and size of river captures (Fig. 6 c).



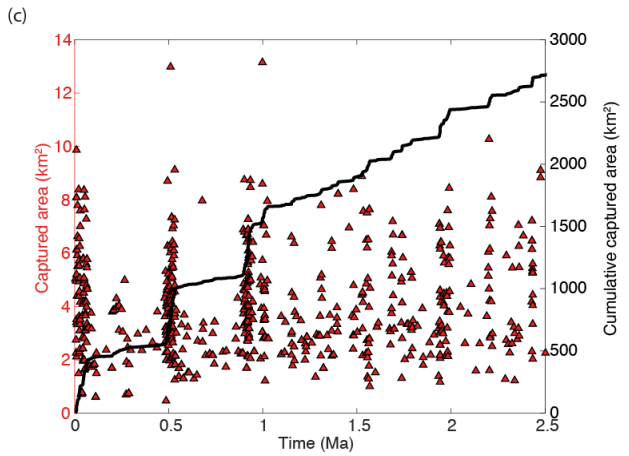
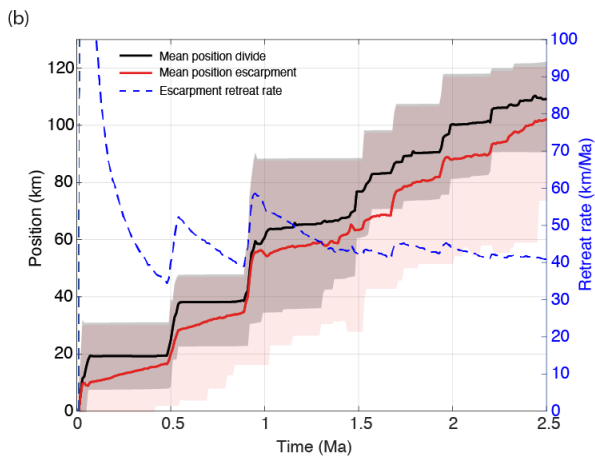
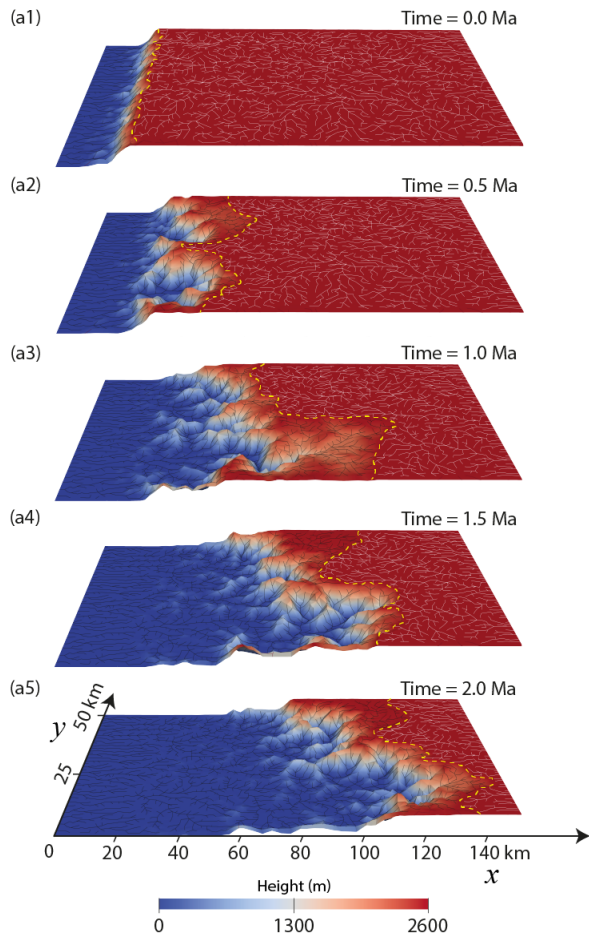
213

214 Fig. 6 Results of the homogeneous substrate model of simulation S0. Model dimensions are 100 km in y-
 215 direction and 150 km in the x-direction. The landscape and river network is shown every 1.5 Ma (a1-a5),
 216 although we note that time scales directly with K_b for this model. Escarpment rivers (in black) flow to the
 217 left boundary, which are separated by the major water divide (dashed in yellow) with plateau rivers (in
 218 white) that flow to the right boundary. (b) Mean position of the major divide and the escarpment shows the
 219 near coincidence between the two features in space. The grey and red shading indicate the min and max
 220 positions of the divide and escarpment, respectively. The dashed blue line indicates the retreat rate of the
 221 escarpment. (c) Individual capture events are indicated with their drainage area. The solid black line marks
 222 the cumulative captured area. See Supplement Tables S1, S2 for the parameters of this simulation.

223 3.3 Results of escarpment retreat with a weak surface layer

224 To make direct comparisons of the topographic morphology and retreat rates, we construct simulation S1.
225 The initial condition of S0 and S1 are identical (Fig. 6 a1 and Fig. 7 a1). All model parameters are identical,
226 except for the erodibility of the surface layer; below this weaker, more erodible, surface layer the substrate
227 is the same as simulation S0. Other input parameters are summarized in Supplement Tables S1 and S2.

228 The contrast between the models with and without a weak layer is clear. The weak layer results in an
229 escarpment that retreats faster and is more sinuous (Supplement Movie S3). River capture events are more
230 common and larger, systematically creating a spatial offset between the steep escarpment front and the
231 water divide (Fig. 7 a1-a5, Supplement Movie S2). Many of the river captures are not single events, but are
232 represented by a sequence of captures, where an initial capture or reversal leads to other captures due to
233 rapid incision into the weak surface layer. The mean spatial offset between the divide and the escarpment
234 fluctuates but is maintained at an approximately constant mean distance once the system stabilizes, and
235 therefore the escarpment retreats at a constant rate and maintains the stepped, knickzone-type river profile
236 that would be regarded as typical for an arch-type margin (Fig. 7 b). Along the strike of the escarpment,
237 retreat rates vary spatially in that the escarpment is sinuous and embayments and salients are observed (Fig.
238 7 a2). Erosional remnants are also formed when the main escarpment has swept past but not fully eroded
239 all bedrock (Fig. 7 a3-a5). The divide-escarpment system retreats at a near-steady rate but there are
240 fluctuations in the rate due to larger river captures.



243 Fig. 7 Results of simulation S1 for an escarpment with a weak surface layer. The landscape and river
 244 network is shown every 0.5 Ma (a1-a5). A spatial offset between divide and escarpment is common due to
 245 the higher frequency and size of capture events, relative to model S0. (b) The mean positions of the main
 246 divide and the escarpment show the systematic offset between the two features in space. The grey and red
 247 shading indicate the min and max positions of the divide and escarpment, respectively. The dashed blue
 248 line indicates the retreat rate of the escarpment. (c) Individual capture events are indicated according to
 249 their drainage area. The solid black line marks the cumulative captured area. See Supplement Tables S1,
 250 S2 for the parameters of this simulation.

251 3.4 Parametric controls on retreat rate

252 The existence of the weak surface layer affects the retreat rate as well as the morphology of the escarpment.
253 To investigate how these characteristics depend on the model parameters, we ran a series of models varying
254 the important parameters, including the plateau height, the erodibility of the surface layer, K_w , and its
255 thickness, T_{hw} . For each model we tracked the important characteristics, including the retreat rate and
256 frequency, and area involved in river captures.

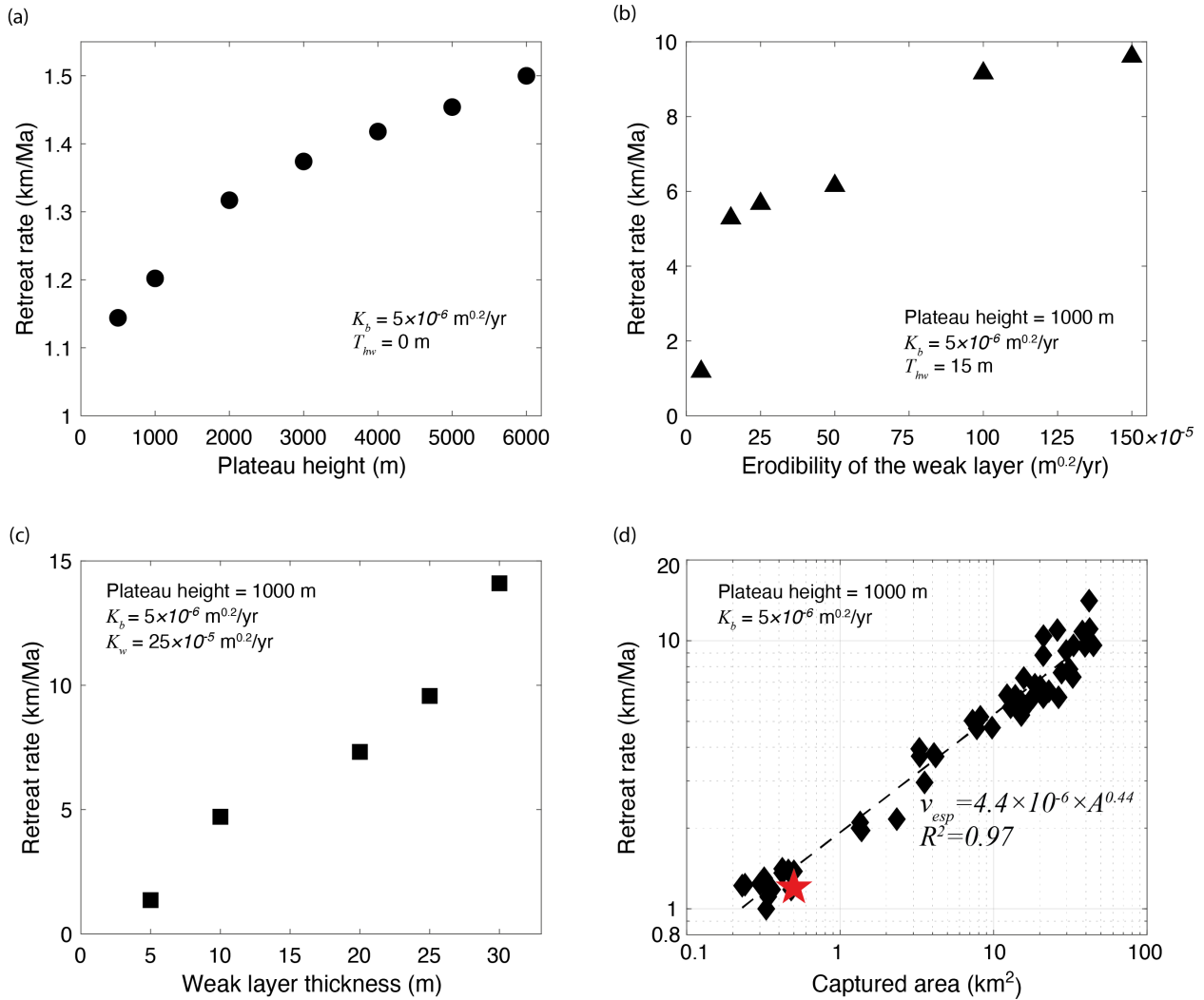
257 Plateau or escarpment height provides the potential energy for erosional processes, so it has been argued
258 that retreat rate should scale with height (Willett et al., 2018). We have confirmed this result by conducting
259 7 simulations using the same initial river pattern and homogeneous erodibility as in model S0, but varying
260 the plateau height (simulations S2-S8) (Figure 8a). These models were run until a dynamic steady retreat
261 rate was achieved. (Supplement Movie S4). These models provide a comparative baseline for the weak
262 layer models.

263 The basement erodibility, K_b , also provides a direct scaling of the retreat rate for the homogeneous models
264 (Willett et al., 2018). With the linear ($n=1$) stream power model, and homogeneous material, model time
265 scales directly with K_b , so there is a direct and linear dependence on erodibility, assuming time-independent
266 hillslope processes. For the weak-layer models, we express the erodibility of the weak layer as a ratio to the
267 basement erodibility, noting that results will all scale with K_b .

268 The existence of the weak surface layer increases the retreat velocity by increasing the frequency and size
269 of river captures. By capturing upstream drainage area, the discharge over the steep escarpment increases
270 along with the incision rate and thus the retreat rate. A weak surface layer increases the plateau drainage
271 area and the area at any given time will be larger with a more erodible layer (Fig. 8b) or a thicker layer (Fig.
272 8c). The parametric relationship between the weak layer and the retreat rate can be generalized by plotting
273 retreat rate against the area above the escarpment (Fig. 8d). This collapses all model results onto a single
274 scaling relationship.

275

276



277

278 Fig. 8 Parametric dependence of escarpment retreat rates in numerical models. (a) Retreat rate against
 279 plateau height for a homogeneous erodibility (simulations S2-S8). (b) Effect of erodibility of surface layer
 280 of constant thickness (simulations S9-S14). (c) Effect of surface layer thickness with a fixed erodibility
 281 contrast of K_w/K_b (simulations S15-S19). (d) Combined effects of surface layer thickness and erodibility
 282 expressed through the instantaneous drainage area above the escarpment of constant plateau height. Black
 283 diamonds are from simulations S9-S19 of the weak surface layer model. The red star is from simulation S3
 284 of the homogeneous substrate model. The regression (dashed line) of the retreat rate, V_{esp} (m/yr) and

285 captured area, A (m^2) is shown. See Supplement Tables S3 and S4 for the parameters of simulations S2-
286 S19.

287 4 Discussion

288 4.1 Retreat rate and morphology of escarpment river profiles during retreat

289 Our models demonstrated that a knickzone-type escarpment whereby river profiles show a distinct
290 morphological step at the escarpment face, but an inland water divide can emerge through processes of
291 escarpment and divide migration with a heterogeneous substrate. A more erodible surface layer, such as
292 occurs through weathering of crustal rocks can predispose an escarpment to large or frequent river captures
293 and thus higher occurrence of stepped river profiles. With a surface layer that has sufficient thickness and
294 weak rock strength, the divide migrates through discrete captures and reversals of plateau rivers at rates
295 that are sufficiently fast to maintain a significant distance with the escarpment, and therefore, maintaining
296 the stepped shape of the escarpment-divide system during retreat.

297 A key model observation is that although the escarpment and water divide evolve into a statistically
298 stationary form with a constant separation distance, this is only a statistical relationship and individual
299 rivers will deviate from the mean. In particular, any given margin, or even a specific drainage basin may
300 exhibit both stepped- and unstepped river profiles (e.g. eastern Madagascar in Figure 2 and the conjugate
301 margin of western India in Supplement Figure S4), depending on the history of river capture in the upstream
302 reaches. This is a consequence of the discrete nature of divide migration through river capture. The dendritic
303 nature of the plateau river network also affects the geometry of the drainage basins and the frequency and
304 size of captures. Water divides with head-to-head river valleys exhibit more gradual divide migration whilst
305 rivers head-to-trunk lead to more discrete captures (Bishop, 1995). Discrete captures bring additional
306 erosional power to the escarpment, and therefore drive the escarpment retreat rate at a higher rate. However,
307 depending on the relative rate of the escarpment retreat and the water divide, the plateau area may either

308 increase or decrease, leading to transience in the escarpment retreat rate. In extreme cases, the divide-
309 escarpment system can oscillate between the knickzone-type and the divide-type due to discrete capture-
310 driven divide migration, followed by escarpment retreat bringing the escarpment to the water divide.
311 Collectively, the escarpment-divide retreat system is a 2D problem that can exhibit considerable variability
312 in both space and time.

313 The common occurrence of two types of escarpment-draining rivers across the escarpment of Madagascar
314 (Fig. 2) supports this model for the formation of stepped, knickzone-type profiles. The fact that both types
315 of rivers coexist along the escarpments of Madagascar suggests that the escarpment morphology is not a
316 characteristic of the uplift pattern, but represents a perpetual state of a divide-escarpment migration with a
317 large average distance between the escarpment and the water divide. Given the weathered plateau surface
318 of Madagascar (Cox et al., 2010; Wells et al., 1997; Wells and Andriamihaja, 1993, 1990) and established
319 river capture events near the major divide, we suggest that the current morphology reflects the retreat of the
320 escarpment-divide system through progressive, discrete capture of the high plateau, and that this process
321 has been active since continental rifting (Braun, 2018; Wang et al., 2021; Wang and Willett, 2021).

322 Although river captures occur on divide-type escarpments, the occurrence of a weak surface layer on the
323 upper plateau greatly increases the frequency and size of captures. The increase is largely the result of
324 complex, sequential captures. For example, the pattern of headward piracy, whereby a major river is
325 reversed and all its tributaries captured is encouraged by an erodible surface layer (Harel et al., 2019). This
326 sequence occurs frequently in the numerical models as well as in Madagascar as demonstrated by the
327 Mananara and Manampatrana examples (Fig. 3). From the model observations, a thicker and weaker surface
328 layer is prone to drive faster divide migration and therefore faster escarpment migration. The overall impact
329 of the weak surface layer on retreat rate can be directly expressed by the captured area which we show
330 scales positively with retreat rate (Fig. 8d). The capture history of individual escarpment rivers or
331 catchments is complex and retreat rates unsteady; the captured area, however, provides a snapshot of the
332 current retreat rate which can be tested with natural data.

333 Within this framework, the distinction between divide-type escarpment rivers and knickzone-type
334 escarpment rivers can be seen as artificial. All escarpments migrate by divide migration, river reversal and
335 capture, but with differing degrees of transience. A divide-type escarpment river profile can be seen as the
336 end-member mode where, at least locally, no river capture has occurred in the recent past. If an escarpment
337 shows a predominance of divide-type rivers, it is an indication that conditions are not optimal for reversals
338 and captures, e.g. no weathered weak layer, or the river pattern on the upper surface is not favorable for
339 river capture. The counter case, where a margin escarpment shows dominantly stepped profiles, may reflect
340 conditions favourable to river reversal and capture, rather than a fundamental difference in uplift pattern,
341 i.e. arching of the passive margin. Given that river capture accelerates retreat rates, the divide-type rivers
342 represent a “background” retreat rate. This background rate will scale with plateau height and rock
343 erodibility (e.g. Willett et al., 2018), but will be locally enhanced wherever river capture occurs
344 (Supplement Movie S5). This enhancement should follow a scaling with captured area (Fig. 8d).

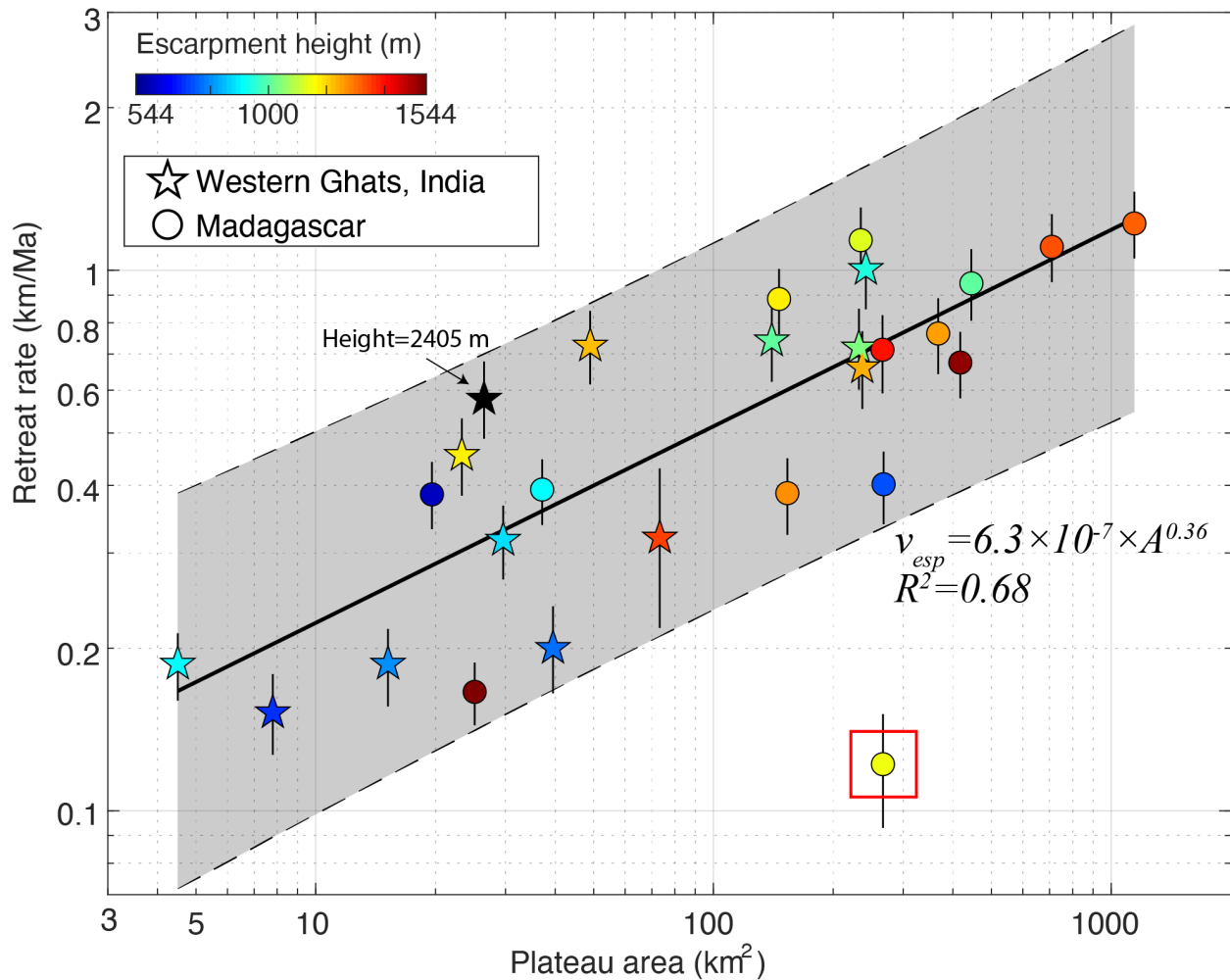
345 4.2 Comparison with the escarpments of Madagascar and the Western Ghats of India

346 Madagascar and the Western Ghats of India represent conjugate margins (Thompson et al., 2019), each of
347 which is characterized by a large escarpment. The climate of the two escarpments is similar with both
348 dominated by monsoonal and orographic precipitation (Gunnell, 1997; Scroxton et al., 2017; Varikoden et
349 al., 2019). The lithology of the two escarpments is primarily Precambrian metamorphic rock. Studies show
350 that the Deccan plateau inland of the great escarpment of the Western Ghats in India is highly weathered
351 as we inferred for Madagascar (Beauvais et al., 2016; Bonnet et al., 2016, 2014). Both knickzone-type and
352 divide-type escarpment river profiles are found in the Western Ghats. About 33% of the escarpment rivers
353 of the Western Ghats show knickzone-type or indeterminate morphology (Supplement Figure S4). We test
354 the scaling relationship of retreat rate and drainage area with the DCN ^{10}Be concentration-derived retreat
355 rates of both the Madagascar escarpment and the Western Ghats using the results of Wang et al. (2021).
356 We select escarpment-draining basins with a significant portion of plateau area. This is complicated by the

357 fact that an escarpment-draining basin can have multiple tributary rivers that originate from the plateau but
358 have a variable area above the escarpment edge.

359 DCN ^{10}Be concentration-derived retreat rates of the Madagascar escarpment and the Western Ghats
360 escarpment positively scale with the drainage area above the escarpment edge (Fig. 9). One basin (marked
361 with a red open box) deviates from the trend, and has an unusual morphology with deep and narrow gorges
362 and significant captured plateau area but minimal lowland area, leading to large uncertainty in the derived
363 retreat rate (Wang and Willett, 2021). Taking out this outlier basin, the remaining data show a statistically
364 strong correlation ($p < 0.001$ for the regression in log-log space).

365 The remaining variability in retreat rate can be partially explained by variability in plateau height and rock
366 erodibility of the escarpment. The plateau height of Madagascar and India escarpment covers a wide range
367 of 500 m-2500 m (Fig. 9). Although there is not a clear correlation between height and retreat rate, some
368 large residuals seem to be related to height variations (Fig. 9). Given the heterogeneity of the escarpment
369 substrate, rock erodibility could also explain some of the variance in Figure 9. Although the primary
370 lithology of both margins is Precambrian metamorphic rock, a variety of lithology is present in different
371 individual basins and there is some variance reduction by considering specific rock types in the catchments
372 (Supplement Figure S5).



374

375 Fig. 9 Measured retreat rates of the Madagascar escarpment and the Western Ghats escarpment from detrital
 376 cosmogenic nuclide ¹⁰Be concentrations. Regression omitting one outlier for retreat rate, V_{esp} (m/yr), and
 377 captured area, A (m²) is shown. Measured escarpment retreat rates from Wang et al. (2021). Grey shading
 378 is the 95% confidence envelope.

379 5 Conclusions

380 In this paper, we have used theory, numerical models, geomorphological and geochemical data to support
 381 the idea that the morphological difference in escarpment river profiles, in particular, the spatial offset

382 between the main water divide and escarpment is a consequence of river captures that occur as the
383 escarpment migrates. Escarpments are characterized by rivers that head against the escarpment and others
384 that drain part of the upper plateau. We argue that the relative proportion of each type depends on the ease
385 with which river capture occurs and thus the size and frequency of captures. Large and frequent captures
386 are particularly encouraged by a more easily eroded upper surface of the plateau, a condition that we argue
387 is present in Madagascar and the Western Ghats of India due to surface weathering. High surface weathering
388 is encouraged by the warm, wet climate and low physical erosion rates of the highlands. Our 2D landscape
389 evolution models confirmed the hypothesis and revealed a power-law scaling between the retreat rate and
390 the captured area. The retreat rates of the great escarpments of Madagascar and India are consistent with
391 this hypothesized scaling.

392 Code availability

393 Codes of the landscape evolution models are available at [https://github.com/yanyanwangesd/DAC-](https://github.com/yanyanwangesd/DAC-weaksurfacelayer)
394 [weaksurfacelayer](https://github.com/yanyanwangesd/DAC-weaksurfacelayer) or upon request to the corresponding author.

395

396 References

397 Beauvais, A., Bonnet, N.J., Chardon, D., Arnaud, N., Jayananda, M., 2016. Very long-term stability of
398 passive margin escarpment constrained by $^{40}\text{Ar}/^{39}\text{Ar}$ dating of K-Mn oxides. *Geology* 44, 299–302.
399 <https://doi.org/10.1130/G37303.1>

400 Bishop, P., 2007. Long-term landscape evolution: linking tectonics and surface processes. *Earth Surf.*
401 *Process. Landforms* 32, 329–365. <https://doi.org/10.1002/esp>

402 Bishop, P., 1995. Drainage rearrangement by river capture, beheading and diversion. *Progress in Physical*
403 *Geography: Earth and Environment* 19, 449–473. <https://doi.org/10.1177/030913339501900402>

404 Bonnet, N.J., Beauvais, A., Arnaud, N., Chardon, D., Jayananda, M., 2016. Cenozoic lateritic weathering
405 and erosion history of Peninsular India from $^{40}\text{Ar}/^{39}\text{Ar}$ dating of supergene K–Mn oxides. *Chemical*
406 *Geology* 446, 33–53. <https://doi.org/10.1016/j.chemgeo.2016.04.018>

407 Bonnet, N.J., Beauvais, A., Arnaud, N., Chardon, D., Jayananda, M., 2014. First $^{40}\text{Ar}/^{39}\text{Ar}$ dating of
408 intense Late Palaeogene lateritic weathering in Peninsular India. *Earth and Planetary Science Letters*
409 386, 126–137. <https://doi.org/10.1016/j.epsl.2013.11.002>

410 Braun, J., 2018. A review of numerical modeling studies of passive margin escarpments leading to a new
411 analytical expression for the rate of escarpment migration velocity. *Gondwana Research*.
412 <https://doi.org/10.1016/j.gr.2017.04.012>

413 Brosens, L., Broothaerts, N., Campforts, B., Jacobs, L., Razanamahandry, V.F., van Moerbeke, Q., Bouillon,
414 S., Razafimbelo, T., Rafolisy, T., Govers, G., 2022. Under pressure: Rapid lavaka erosion and
415 floodplain sedimentation in central Madagascar. *Science of the Total Environment* 806.
416 <https://doi.org/10.1016/j.scitotenv.2021.150483>

417 Cox, R., Zentner, D.B., Rakotondrazafy, A.F.M., Rasoazanamparany, C.F., 2010. Shakedown in
418 Madagascar: Occurrence of lavakas (erosional gullies) associated with seismic activity. *Geology* 38,
419 179–182. <https://doi.org/10.1130/G30670.1>

420 Davies, J., 2009. Hydrogeological mapping of north-central Madagascar using limited data. *Groundwater*
421 2009 conference, Cape Town.

422 de Sordi, M.V., Salgado, A.A.R., Siame, L., Bourlès, D., Paisani, J.C., Léanni, L., Braucher, R., do Couto,
423 E.V., 2018. Implications of drainage rearrangement for passive margin escarpment evolution in
424 southern Brazil. *Geomorphology* 306, 155–169. <https://doi.org/10.1016/j.geomorph.2018.01.007>

425 Delaunay, A., 2018. The vertical movements of Madagascar (90–0 Ma): A coupled analysis of the
426 landforms and the dimensional recording of the western Malagasy margins. *Rennes 1*.

427 Gallen, S.F., 2018. Lithologic controls on landscape dynamics and aquatic species evolution in post-
428 orogenic mountains. *Earth and Planetary Science Letters* 493, 150–160.
429 <https://doi.org/10.1016/j.epsl.2018.04.029>

430 Giachetta, E., Willett, S.D., 2018. Effects of river capture and sediment flux on the evolution of plateaus:
431 Insights from numerical modeling and river profile analysis in the upper blue Nile catchment. *Journal*
432 *of Geophysical Research: Earth Surface* 123, 1187–1217. <https://doi.org/10.1029/2017JF004252>

433 Goren, L., Willett, S.D., Herman, F., Braun, J., 2014. Coupled numerical-analytical approach to landscape
434 evolution modeling. *Earth Surface Processes and Landforms* 39, 522–545.
435 <https://doi.org/10.1002/esp.3514>

436 Gunnell, Y., 1997. Relief and climate in South Asia: the influence of the Western Ghats on the current
437 climate pattern of peninsular India. *International journal of climatology: a journal of the Royal*
438 *Meteorological Society* 17, 1169–1182. [https://doi.org/10.1002/\(SICI\)1097-
439 0088\(199709\)17:11<1169::AID-JOC189>3.0.CO;2-W](https://doi.org/10.1002/(SICI)1097-0088(199709)17:11<1169::AID-JOC189>3.0.CO;2-W)

440 Gunnell, Y., Harbor, D., 2008. Structural Underprint and Tectonic Overprint in the Angavo (Madagascar)
441 and Western Ghats (India)-Implications for Understanding Scarp Evolution at Passive Margins.
442 *JOURNAL GEOLOGICAL SOCIETY OF INDIA* 71, 763–779.

443 Guo, Y., Yang, S., Su, N., Li, C., Yin, P., Wang, Z., 2018. Revisiting the effects of hydrodynamic sorting
444 and sedimentary recycling on chemical weathering indices. *Geochimica et Cosmochimica Acta* 227,
445 48–63. <https://doi.org/10.1016/j.gca.2018.02.015>

446 Harel, E., Goren, L., Shelef, E., Ginat, H., 2019. Drainage reversal toward cliffs induced by lateral lithologic
447 differences. *Geology* 47, 928–932. <https://doi.org/10.1130/G46353.1>

448 Harnois, L., 1988. The CIW index: a new chemical index of weathering. *Sediment Geol* 55, 319–322.

449 Jarvis, A., Reuter, H.I., Nelson, A., Guevara, E., 2008. Hole-filled seamless SRTM data, Version 4,
450 International Centre for Tropical Agriculture (CIAT).

451 Kirby, E., Whipple, K.X., 2012. Expression of active tectonics in erosional landscapes. *Journal of Structural*
452 *Geology*. <https://doi.org/10.1016/j.jsg.2012.07.009>

453 Kooi, H., Beaumont, C., 1994. Escarpment evolution on high-elevation rifted margins: Insights derived
454 from a surface processes model that combines diffusion, advection, and reaction. *Journal of*
455 *Geophysical Research: Solid Earth* 99, 12191–12209. <https://doi.org/10.1029/94JB00047>

456 Lecomte, P.J.D.A.I.P.K.L., 2014. Weathering and the Riverine Denudation of Continents, *SpringerBriefs*
457 *in Earth System Sciences*. <https://doi.org/10.1007/978-94-007-7717-0>

458 Lehner, B., Verdin, K., Jarvis, A., 2008. New global hydrography derived from spaceborne elevation data.
459 *Eos, Transactions American Geophysical Union* 89, 93–94.

460 Matmon, A., Bierman, P., Enzel, Y., 2002. Pattern and tempo of great escarpment erosion, *Geology*.
461 [https://doi.org/10.1130/0091-7613\(2002\)030<1135:PATOGE>2.0.CO;2](https://doi.org/10.1130/0091-7613(2002)030<1135:PATOGE>2.0.CO;2)

462 Perron, J.T., Royden, L., 2013. An integral approach to bedrock river profile analysis. *Earth Surface*
463 *Processes and Landforms* 38, 570–576. <https://doi.org/10.1002/esp.3302>

464 Prince, P.S., Spotila, J.A., Henika, W.S., 2010. New physical evidence of the role of stream capture in
465 active retreat of the Blue Ridge escarpment, southern Appalachians. *Geomorphology* 123, 305–319.
466 <https://doi.org/10.1016/j.geomorph.2010.07.023>

467 Rahobisoa, J.J., Rajaobelison, J., Schuth, C., Kallioras, A., Ramaroson, V., 2014. Use of isotopic signatures
468 for the determination of natural recharge and chemical characterization of groundwaters: The case of
469 Horombe plateau area, SW Madagascar. *Environmental Earth Sciences* 71, 4497–4511.
470 <https://doi.org/10.1007/s12665-013-2842-9>

471 Rudnick, R.L., Gao, S., 2005. Composition of the Continental Crust, in: Rudnick, R.L. (Ed.), *The Crust*.

472 Schreurs, G., Giese, J., Berger, A., Gnos, E., 2010. A new perspective on the significance of the Ranotsara
473 shear zone in Madagascar. *International Journal of Earth Sciences* 99, 1827–1847.
474 <https://doi.org/10.1007/s00531-009-0490-9>

475 Scroxtton, N., Burns, S.J., McGee, D., Hardt, B., Godfrey, L.R., Ranivoharimanana, L., Faina, P., 2017.
476 Hemispherically in-phase precipitation variability over the last 1700 years in a Madagascar
477 speleothem record. *Quaternary Science Reviews* 164, 25–36.
478 <https://doi.org/10.1016/j.quascirev.2017.03.017>

479 Thompson, J.O., Moulin, M., Aslanian, D., de Clarens, P., Guillocheau, F., 2019. New starting point for
480 the Indian Ocean: Second phase of breakup for Gondwana. *Earth-Science Reviews*.
481 <https://doi.org/10.1016/j.earscirev.2019.01.018>

482 Tucker, G.E., Slingerland, R.L., 1994. Erosional dynamics, flexural isostasy, and long-lived escarpments:
483 A numerical modeling study. *Journal of Geophysical Research: Solid Earth* 99, 12229–12243.
484 <https://doi.org/10.1029/94JB00320>

485 Tucker, R.D., Roig, J.Y., Moine, B., Delor, C., Peters, S.G., 2014. A geological synthesis of the
486 Precambrian shield in Madagascar. *Journal of African Earth Sciences* 94, 9–30.
487 <https://doi.org/10.1016/j.jafrearsci.2014.02.001>

488 Varikoden, H., Revadekar, J. v, Kuttippurath, J., Babu, C.A., 2019. Contrasting trends in southwest
489 monsoon rainfall over the Western Ghats region of India. *Climate Dynamics* 52, 4557–4566.
490 <https://doi.org/10.1007/s00382-018-4397-7>

491 Wang, Y., Willett, S.D., 2021. Escarpment retreat rates derived from detrital cosmogenic nuclide
492 concentrations. *Earth Surface Dynamics* 9, 1301–1322. <https://doi.org/10.5194/esurf-9-1301-2021>

493 Wang, Y., Willett, S.D., Wu, D., Haghypour, N., Christl, M., 2021. Retreat of the Great Escarpment of
494 Madagascar From Geomorphic Analysis and Cosmogenic ¹⁰ Be Concentrations. *Geochemistry,*
495 *Geophysics, Geosystems* 22. <https://doi.org/10.1029/2021GC009979>

496 Wells, N.A., Andriamihaja, B., 1993. The initiation and growth of gullies in Madagascar: are humans to
497 blame? [https://doi.org/10.1016/0169-555X\(93\)90002-J](https://doi.org/10.1016/0169-555X(93)90002-J)

498 Wells, N.A., Andriamihaja, B., 1990. Evidence for cryptic colluvial addition and removal at the tops of
499 laterite profiles in Madagascar / Mise en évidence d'apport et d'ablation de colluvions cryptiques au
500 sommet de profils latéritiques de Madagascar. *Sciences Géologiques. Bulletin* 43, 237–251.
501 <https://doi.org/10.3406/sgeol.1990.1858>

502 Wells, N.A., Andriamihaja, B., Goodman, S.M., Patterson, B.D., 1997. Extreme gully erosion in
503 Madagascar and its natural and anthropogenic causes. *Natural change and human impact in*
504 *Madagascar* 44–47.

505 Whipple, K.X., Tucker, G.E., 1999. Dynamics of the stream-power river incision model: Implications for
506 height limits of mountain ranges, landscape response timescales, and research needs. *Journal of*
507 *Geophysical Research: Solid Earth* 104, 17661–17674. <https://doi.org/10.1029/1999jb900120>

508 Willett, S.D., McCoy, S.W., Beeson, H.W., 2018. Transience of the North American High Plains landscape
509 and its impact on surface water. *Nature* 561, 528–532. <https://doi.org/10.1038/s41586-018-0532-1>

510 Wobus, C., Whipple, K.X., Kirby, E., Snyder, N., Johnson, J., Spyropolou, K., Crosby, B., Sheehan, D.,
511 2006. Tectonics from topography: Procedures, promise, and pitfalls. *Special Paper of the Geological*
512 *Society of America* 398, 55–74. [https://doi.org/10.1130/2006.2398\(04\)](https://doi.org/10.1130/2006.2398(04))

513

Supplement to *Divide migration and escarpment retreat: numerical models and application to the rift margin of Madagascar*

Yanyan Wang¹; Sean D. Willett¹; Datian Wu²

¹ETH Zurich, Department of Earth Sciences, Sonneggstrasse 5, 8092 Zurich, Switzerland.

²China Geological Survey, Shengyang Center, Huanghe North Street 280, 110034 Shenyang, China.

Corresponding author: Yanyan Wang (yanyan.wang@erdw.ethz.ch)

Supplement includes:

- Five supplementary figures
- Four supplement tables
- Five supplement movies

Supplement figures:

- Figure S1 Chemical index of alteration (CIA) from river sediment of Madagascar.
- Figure S2 Plagioclase index of alteration (PIA) from river sediment of Madagascar.
- Figure S3 Weathering index of Parker (WIP) from river sediment of Madagascar.
- Figure S4 Escarpment river types of the southern Western Ghats in India.
- Figure S5 Regressions including rock erodibility of Madagascar and the Western Ghats, India.

Supplement tables:

- Table S1 Fixed default simulation parameters of simulations S0-S1 and S20-S23.
- Table S2 Varying simulation parameters of simulations S0-S1 and S20-S23.
- Table S3 Identical default simulation parameters of simulations S2 to S19.
- Table S4 Varying simulation parameters of simulations S2 to S19.

Supplement movies:

- Movie S1 Model behavior of the homogenous substrate model.
- Movie S2 Model behavior of the weak surface layer model.
- Movie S3 Comparison of a homogenous substrate and weak surface layer models.
- Movie S4 Comparison of the homogenous substrate model with different heights.
- Movie S5 Comparison of the weak surface layer with different heights.

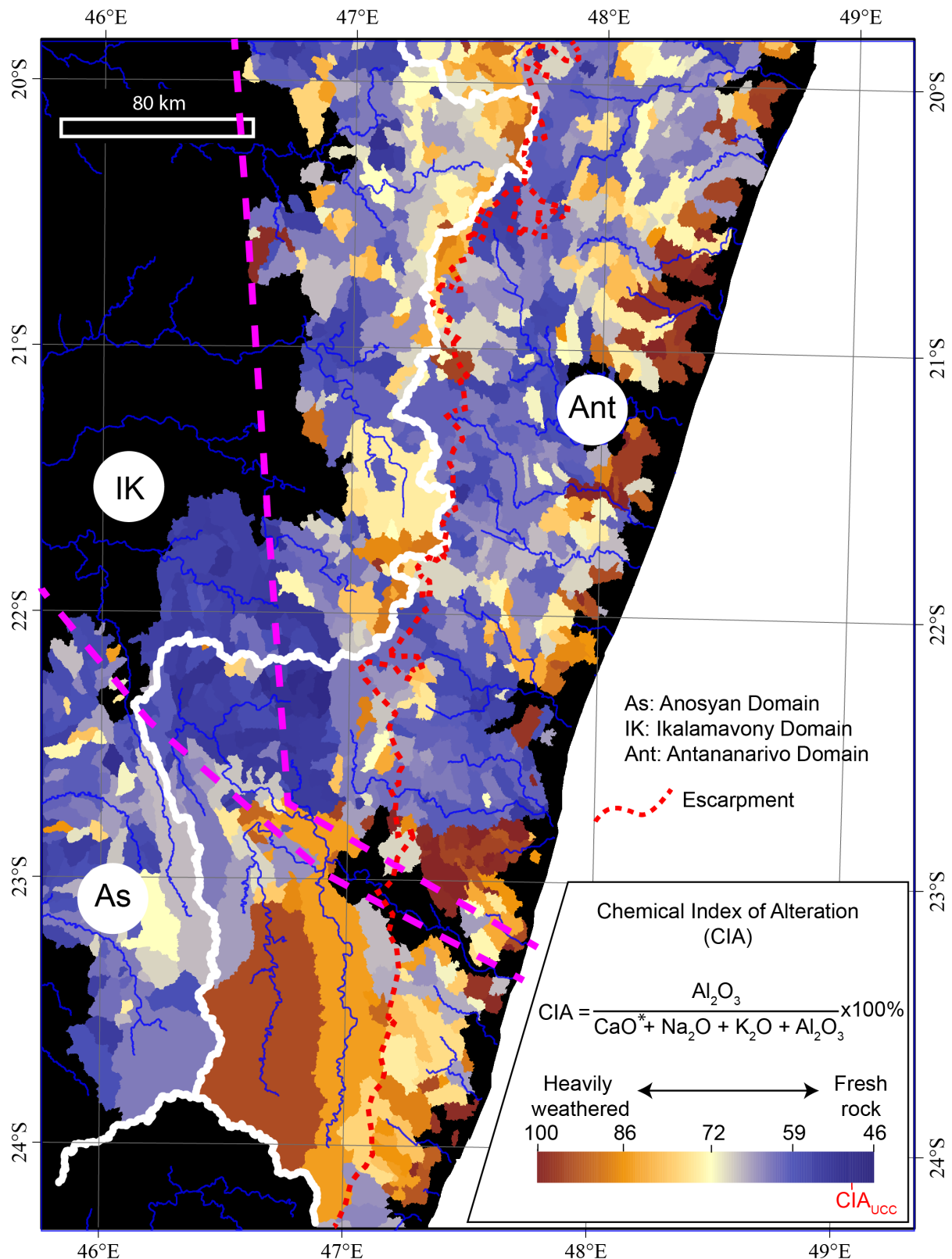


Fig. S1 Chemical index of alteration (CIA, Nesbitt and Young, 1982) from river sediment of Madagascar. High CIA indicates a high degree of weathering. The mean CIA of average elemental compositions of upper continental crust (CIA_{UCC}) is from Rudnick and Gao (2005). The three geological domains (As, IK, and Ant) are indicated and are different in age and major lithological composition (Tucker et al., 2014). Compositional and morphological effects are evident with low CIA in the IK and on the escarpment. Higher values of CIA are observed on both the plateau and the coastal lowlands.

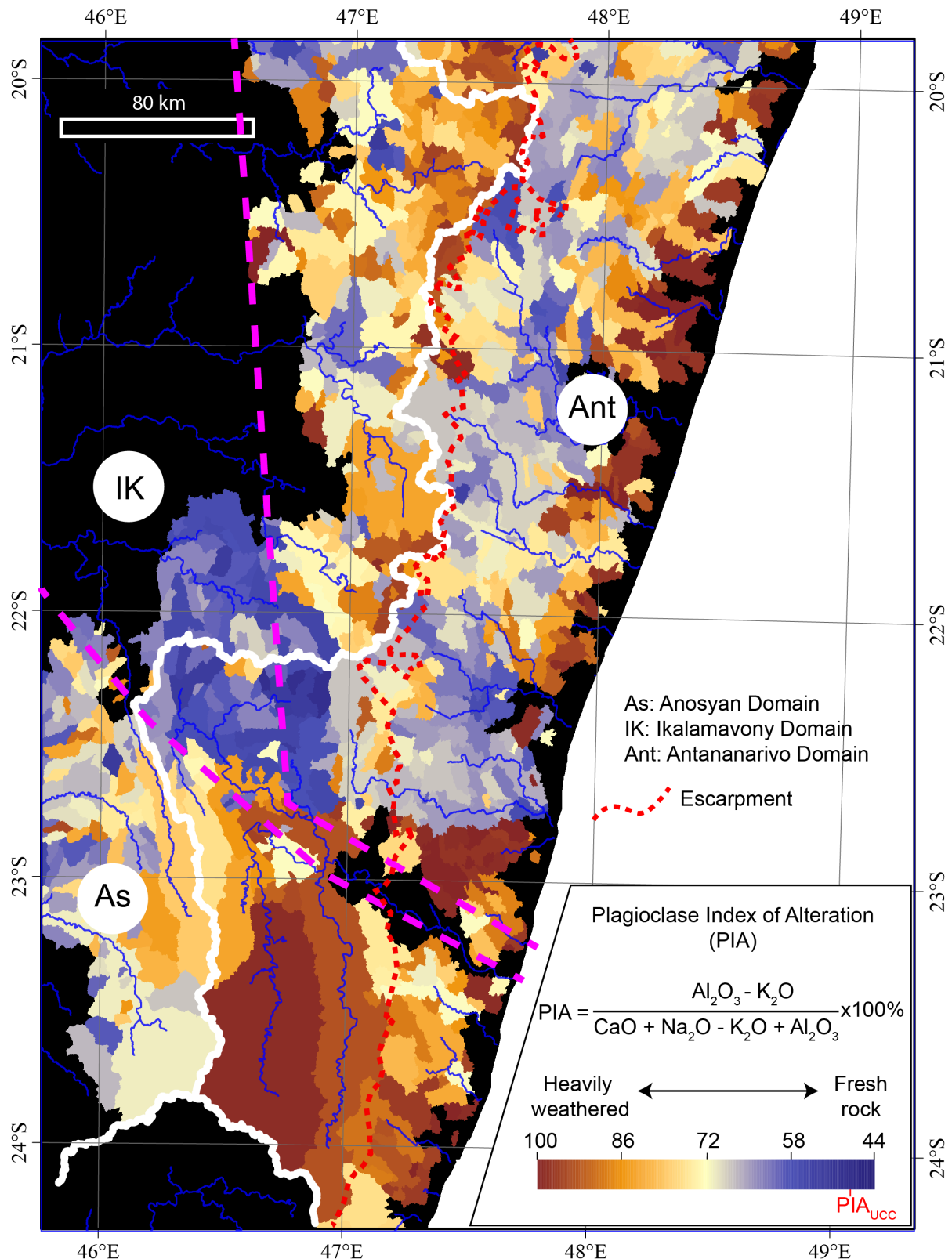


Fig. S2 Plagioclase index of alteration (PIA, Fedo et al., 1995) from river sediment of Madagascar. High PIA indicates a high degree of weathering. The mean PIA of average elemental compositions of upper continental crust (PIA_{UCC}) is from Rudnick and Gao (2005). The three geological domains (As, IK, and Ant) are indicated and are different in age and major lithological composition (Tucker et al., 2014). Compositional and morphological effects are

evident with low PIA in the IK and on the escarpment. Higher values of PIA are observed on both the plateau and the coastal lowlands.

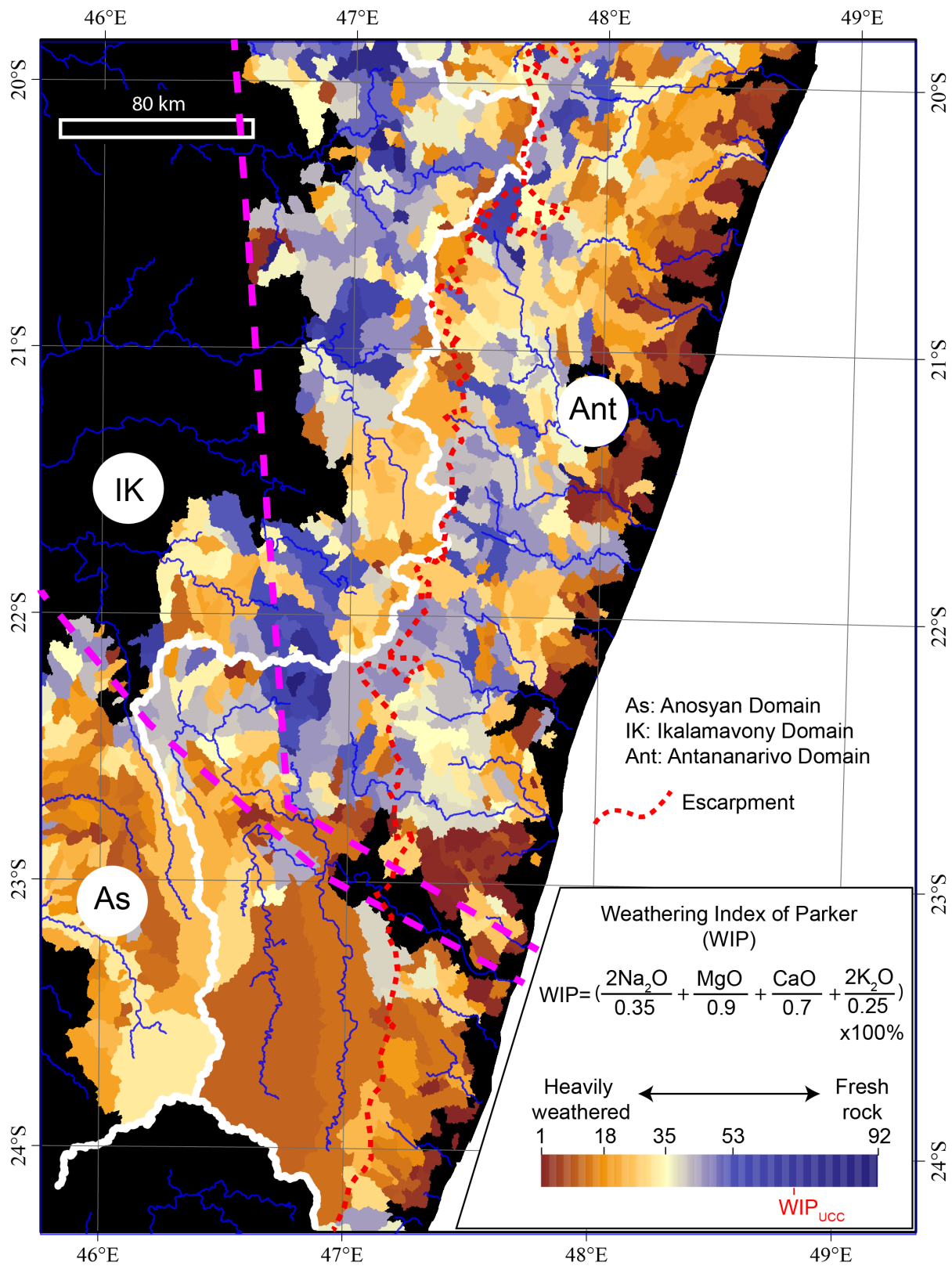


Fig. S3 Weathering index of Parker (WIP, Lecomte, 2014) from river sediment of Madagascar. Low WIP indicates a high degree of weathering. The mean WIP of average elemental

compositions of upper continental crust (WIP_{UCC}) is from Rudnick and Gao (2005). The three geological domains (As, IK, and Ant) are indicated and are different in age and major lithological composition (Tucker et al., 2014). Compositional and morphological effects are evident with high WIP in the IK and on the escarpment. Lower values of WIP are observed on both the plateau and the coastal lowlands.

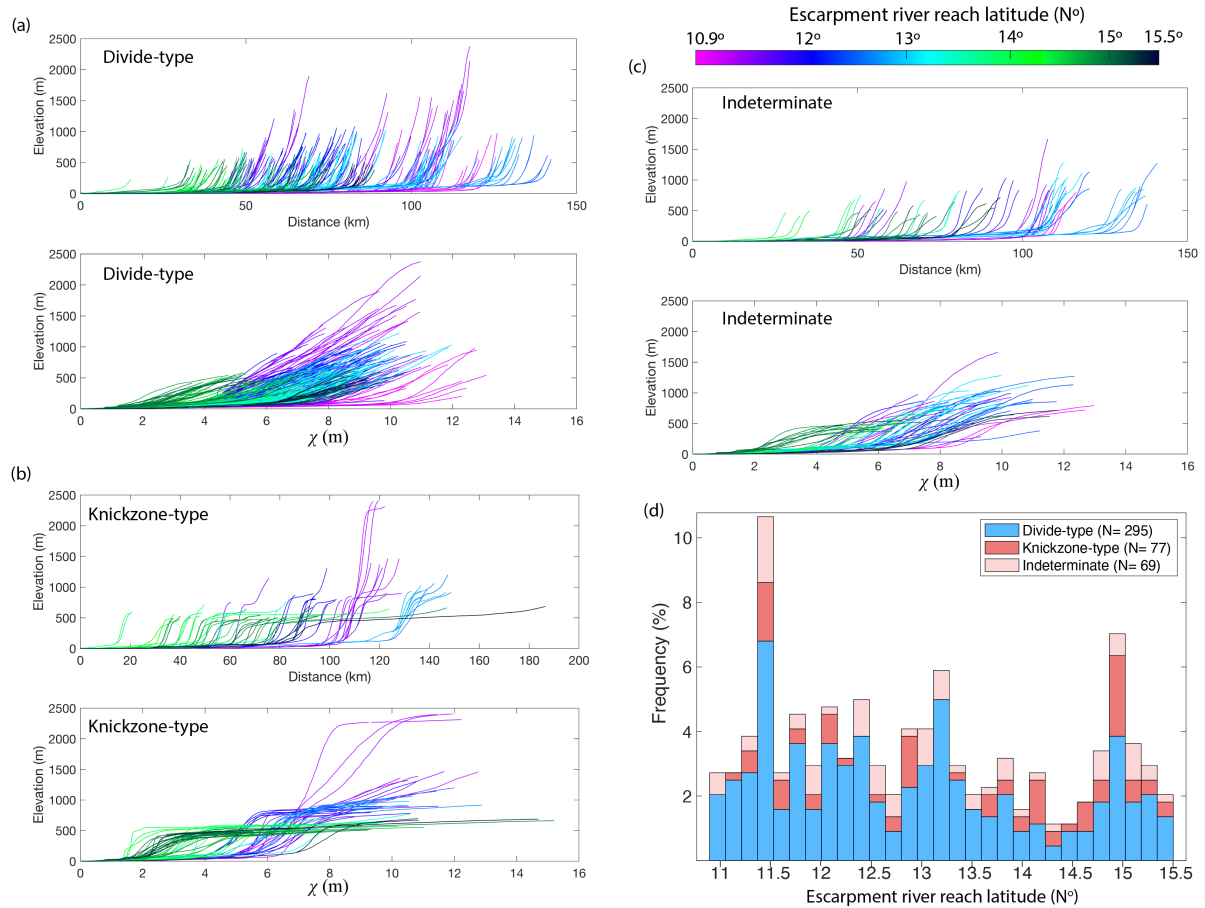


Fig. S4 Escarpment river types of the southern Western Ghats in India where the escarpment develops on the Precambrian basement. (a) Escarpment river profiles exhibiting divide-type, plotted against distance and normalized distance (Perron and Royden, 2013) and colored by the latitude of channel head. (b) Escarpment river profiles exhibiting knickzone-type, plotted in the same manner as (a). (c) Escarpment river profiles of indeterminate form, plotted in the same manner as (a). (d) Spatial variation of escarpment river type along the strike of the great escarpment. The number of escarpment river reaches is shown in the key.

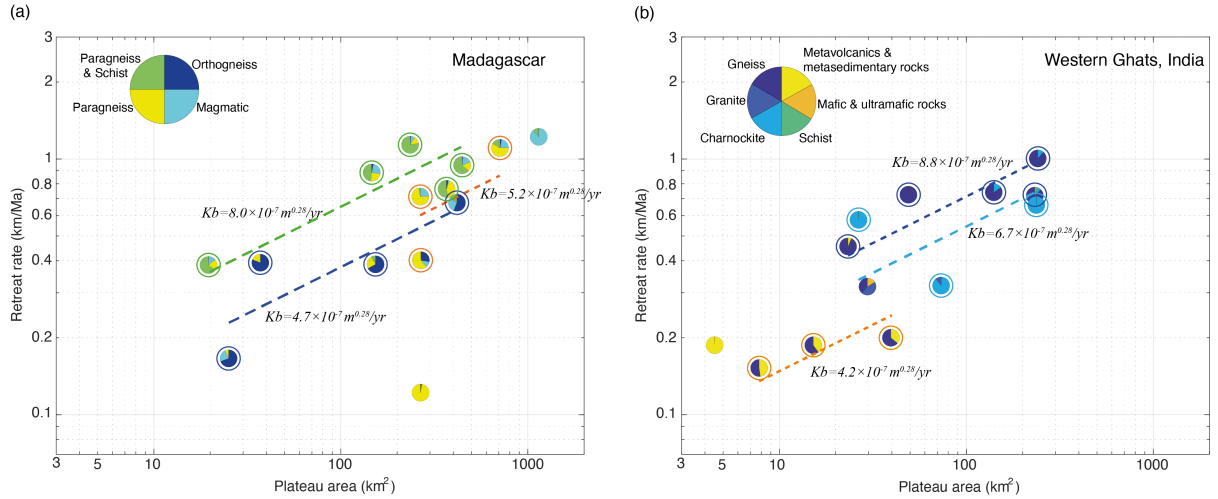


Fig. S5 Regressions of retreat rate, subdivided by substrate type of (a) Madagascar escarpment, (b) Escarpment-draining basins of Western Ghats, India. Each pie chart represents an escarpment basin. The pie chart shows the relative percentage of different rock types. The erodibility of major rock types is calculated by fitting a power exponent of the drainage area of 0.36. Basins used for erodibility calculation are indicated with open circles, colored consistent with the fit (dashed lines). The rock type of Madagascar escarpment is taken from the geological map of Madagascar (Roig et al., 2012). The rock type of Western Ghats escarpment-draining basins is from (Mandal et al., 2015).

Table S1 Fixed default parameters of simulations S0-S1 and S20-S23.

Simulation 0-1 and 20-23	Default parameters	Symbol	Value
	Stream power law slope exponent	n	1
	Stream power law discharge exponent	m	0.495
	Inverse Hack's law power	H	2
	Inverse Hack's law coefficient	k_a	1.66667
	Critical hillslope length	X_c	1000 m
	Critical hillslope angle	θ	21 degree
	Hillslope diffusivity	K_f	0.14 m ² /yr
	Substrate erodibility	K_b	0.000005 m ^{0.2} /yr
	Precipitation rate	p	1 m/yr
	Uniform isostatic uplift rate	U	0.000005 m/yr

Table S2 Varying parameters of simulations S0-S1 and S20-S23.

Simulation number	Plateau height (Z_p , m)	Regolith thickness (T_{hw} , m)	Erodibility ratio (K_w/K_b)
0	2600	0	1
1	2600	10	100
20	3200	10	100
21	3800	10	100
22	4400	10	100
23	5000	10	100

Table S3 Fixed default parameters of simulations S2 to S19.

Simulation 2-19	Default parameters	Symbol	Value
	Stream power law slope exponent	n	1
	Stream power law discharge exponent	m	0.4
	Inverse Hack's law power	H	1.667
	Inverse Hack's law coefficient	k_a	6.7
	Critical hillslope length	X_c	295 m
	Critical hillslope angle	θ	21 degree
	Hillslope diffusivity	K_f	0.14 m ² /yr
	Substrate erodibility	K_b	0.000005 m ^{0.2} /yr
	Precipitation rate	p	1 m/yr
	Uniform isostatic uplift rate	U	0.000005 m/yr

Table S4 Varying parameters of simulations S2 to S19.

Simulation number	Plateau height (Z_p , m)	Regolith thickness (T_{hw} , m)	Erodibility ratio (K_w/K_b)
2	500	0	1
3	1000	0	1
4	2000	0	1
5	3000	0	1
6	4000	0	1
7	5000	0	1
8	6000	0	1
9	1000	15	100
10	1000	15	200
11	1000	15	300
12	1000	15	50
13	1000	15	30
14	1000	15	10
15	1000	5	50
16	1000	10	50
17	1000	20	50
18	1000	25	50
19	1000	30	50

References

- Fedo, C.M., Nesbitt, H.W., Young, G.M., 1995. Unraveling the effects of potassium metasomatism in sedimentary rocks and paleosols, with implications for paleoweathering conditions and provenance. *Geology* 23, 921–924.
- Lecomte, P.J.D.A.I.P.K.L., 2014. *Weathering and the Riverine Denudation of Continents*, SpringerBriefs in Earth System Sciences. <https://doi.org/10.1007/978-94-007-7717-0>
- Mandal, S.K., Lupker, M., Burg, J.P., Valla, P.G., Haghypour, N., Christl, M., 2015. Spatial variability of ¹⁰Be-derived erosion rates across the southern Peninsular Indian escarpment: A key to landscape evolution across passive margins. *Earth and Planetary Science Letters* 425, 154–167. <https://doi.org/10.1016/j.epsl.2015.05.050>

- Nesbitt, Hw., Young, G.M., 1982. Early Proterozoic climates and plate motions inferred from major element chemistry of lutites. *nature* 299, 715–717.
- Perron, J.T., Royden, L., 2013. An integral approach to bedrock river profile analysis. *Earth Surface Processes and Landforms* 38, 570–576. <https://doi.org/10.1002/esp.3302>
- Roig, J.Y., Tucker, R.D., Peters, S.G., Delor, C., Theveniaut, H., 2012. Carte Géologique de la République de Madagascar à 1/1,000,000, Ministère des Mines, Direction de la Géologie, Programme de Gouvernance des Ressources Minérales.
- Rudnick, R.L., Gao, S., 2005. Composition of the Continental Crust, in: Rudnick, R.L. (Ed.), *The Crust*.
- Tucker, R.D., Roig, J.Y., Moine, B., Delor, C., Peters, S.G., 2014. A geological synthesis of the Precambrian shield in Madagascar. *Journal of African Earth Sciences* 94, 9–30. <https://doi.org/10.1016/j.jafrearsci.2014.02.001>